Available online at www.sciencedirect.com

SciVerse ScienceDirect

Acta Materialia 59 (2011) 7125–7134

Acta MATERIALIA

www.elsevier.com/locate/actamat

# Dislocation interactions and low-angle grain boundary strengthening

B. Liu [a,*], D. Raabe [a,*], P. Eisenlohr [a], F. Roters [a], A. Arsenlis [b], G. Hommes [b]

[a] Max-Planck-Institut für Eisenforschung, 40237 Düsseldorf, Germany
[b] Lawrence Livermore National Laboratory, University of California, Livermore, CA 94550, USA

Received 8 April 2011; received in revised form 23 July 2011; accepted 27 July 2011
Available online 22 September 2011

**Abstract**

The transmission of an incoming dislocation through a symmetrical low-angle tilt grain boundary (GB) is studied for $\{110\}\langle 111\rangle$ slip systems in body-centered cubic metals using discrete dislocation dynamics (DD) simulations. The transmission resistance is quantified in terms of the different types of interactions between the incoming and GB dislocations. Five different dislocation interaction types are considered: collinear, mixed-symmetrical junction, mixed-asymmetrical junction, edge junction, and coplanar. Mixed-symmetrical junction formation events are found not only to cause a strong resistance against the incident dislocation penetration, but also to transform the symmetrical low-angle tilt GB into a hexagonal network (a general low-angle GB). The interactions between the incident dislocation and the GB dislocations can form an array of $\langle 100\rangle$ dislocations (binary junctions) in non-coplanar interactions, or a single $\langle 100\rangle$ dislocation in coplanar interaction. We study how the transmission resistance depends on the mobility of $\langle 100\rangle$ dislocations. $\langle 100\rangle$ dislocations have usually been treated as immobile in DD simulations. In this work, we discuss and implement the mobility law for $\langle 100\rangle$ dislocations. As an example, we report how the mobility of $\langle 100\rangle$ dislocations affects the equilibrium configuration of a ternary dislocation interaction.


*Keywords:* Dislocation dynamics; Strength; Dislocation reactions; Dislocation interactions; Low-angle grain boundary

## 1. Introduction

Three-dimensional dislocation dynamics (DD) models [1–6] simulate dislocation motion and multiplication in response to external loading, dislocation interactions (material strength) and track topology evolution of dislocation networks (microstructure). Numerical simulations with these models have profoundly assisted progress in dislocation physics. Madec et al. [7] reported that the strongest dislocation interaction occurs between two dislocations with collinear Burgers vectors gliding on intersecting slip planes. Dislocation multi-junctions were discovered and studied by Bulatov et al. [8]. The size-dependent strengthening frequently observed in micromechanical testing [9] were well explained via new mechanisms observed in DD simulations, namely source-truncation hardening (free surface effect) [10–12] and source-depletion hardening [10,12–14]. Devincre et al. [15] recently made a contribution to the theory of strain hardening by quantifying the dependence of the dislocation mean free path on dislocation interactions, dislocation avalanches, stress state and sample orientation based on DD simulations [16,17].

How dislocation interactions affect the transmission of an incoming dislocation through a symmetrical low-angle tilt grain boundary (GB) (an array of edge dislocations) is investigated in this work for $\{110\}\langle 111\rangle$ slip systems in body-centered cubic (bcc) metals. Five interaction types are considered:

1. Collinear annihilation: two dislocations with collinear Burgers vectors on intersecting slip planes where the screw parts undergo annihilation.
2. Mixed-symmetrical junction: two dislocations with Burgers vectors that are symmetrical with respect to the

* Corresponding authors.
*E-mail addresses:* b.liu@mpie.de (B. Liu), d.raabe@mpie.de (D. Raabe).

1359-6454/$36.00 © 2011 Acta Materialia Inc. Published by Elsevier Ltd. All rights reserved.
doi:10.1016/j.actamat.2011.07.067

intersecting line of their slip planes. A symmetrical junction of mixed character is formed that has a different (1 1 0) slip plane than the parent dislocations.
3. Mixed-asymmetrical junction: two dislocations with Burgers vectors that are asymmetrical with respect to the intersecting line of their slip planes. An asymmetrical junction of mixed character is formed that shares the slip plane with one of the parent dislocations.
4. Edge junction: two dislocations with Burgers vectors that are symmetrical with respect to the intersecting line of their slip planes. A symmetrical junction of edge character is formed that has a (1 0 0) slip plane.
5. Coplanar: two dislocations on the same slip plane with different Burgers vectors. A binary junction is formed with its line direction remaining perpendicular to the slip plane normal of the parent dislocations

When the interactions approach the dislocation core level, one of the three following cases can occur: Burgers vector reaction; formation of bound crossed states; or bypass. Corresponding configurations can be analyzed through simplified self-energy and interaction force balance considerations, or more precisely, be determined directly by DD simulations, see Refs. [18–21]. Specifically, good agreement was found between DD and atomistic simulations for some dislocation core reactions, namely, Lomer–Cottrell locks [22,23], collinear annihilation [7] and ternary junctions [8]. The strengths of these interaction types in the context of mean-field forest hardening can be quantified in terms of the associated interaction coefficients $a^{su}$ of the generalized Taylor relation [24]:

$$\tau_c^s = \mu b \sqrt{\sum_u a^{su} \rho^u},$$

where $\tau_c^s$ is the critical resolved shear stress for slip system $(s)$, $\rho^u$ is the dislocation density on a considered slip system $(u)$, $b$ is the magnitude of the Burgers vector, and $\mu$ is the shear modulus. The interaction coefficients for the binary interactions in bcc metals have been determined by DD simulations [21,25]. In the context of forest hardening, the interaction strengths are averaged over the interacting dislocations of all possible orientations on the two slip systems considered.

In contrast to forest hardening, interactions between an incoming dislocation and dislocations assembled in a low-angle GB have fixed geometries:

- An incoming dislocation touches the GB on the intersection line of its slip plane and the GB plane.
- GB dislocations have energetically favored line orientations (of edge character in the case of a symmetrical low-angle tilt GB).

Thus, the first aspect that we study is how the transmission resistance of the low-angle GB against an incoming dislocation is affected by the different interaction types. The interaction products (binary junction with ⟨1 0 0⟩ Burgers vectors) of free dislocations and GB dislocations could be an array of short dislocation segments in non-coplanar interactions, or a single dislocation in coplanar interaction. We also investigate how the transmission resistance depends on the mobility of ⟨1 0 0⟩ dislocations.

## 2. Dislocation dynamics simulations: methodology

The ParaDiS code (DD code developed at Lawrence Livermore National Laboratory) [6] is used in this work for the numerical simulations. ParaDiS simulates a dislocation network represented by a set of nodes connected by line segments. One stable dislocation node connects a maximum of four segments (arms). Each segment carries a Burgers vector and is assigned a glide plane normal. The conservation of the Burgers vector is assured everywhere in the dislocation network, except at a pinned node with a single arm (e.g. the end points of a Frank–Read source). The force on a dislocation node due to the stress field of its own arms and other segments in the system is calculated based on the non-singular, self-consistent stress field and elastic energy expressions of Cai et al. [26]. The nodal force exerted by external loading is calculated through the Peach–Koehler equation. The nodal velocity is proportional to the projected nodal force by a mobility tensor (see Section 2.2). The topology update of a dislocation network in the ParaDiS code reflects the physics of dislocation motion and collisions in real crystals: Burgers vector reactions (annihilation, junction zipping and unzipping) happen naturally through the collisions and dissociations of dislocation nodes. In what follows, we explain the model aspects that were particularly adapted for this work, mainly concerning the laboratory frame simulation and the mobility law for ⟨1 0 0⟩ dislocations.

### 2.1. Laboratory frame simulation

The simulations of the interactions between an incoming dislocation and a low-angle GB should be conducted in laboratory frames. The normal of the GB plane is chosen as the first sample axis. The intersection line of the slip plane of the incoming dislocation and the GB plane is the second sample axis. The third sample axis is the cross-product of the first two axes. Free dislocations on 12 {1 1 0}⟨1 1 1⟩ slip systems interact with GB dislocations on one of the slip systems in different types: self (1/12), collinear (2/12), mixed-symmetrical junction (2/12), mixed-asymmetrical junction (4/12), edge junction (2/12), and coplanar (1/12). The reference slip systems of the incoming dislocations and the GB dislocations used for the numerical simulations are listed in Table 1, together with the sample frames used for studying the different interactions types.

The current version of ParaDiS public release v. 2.3.5.1 does not support simulations running in a laboratory frame but works in the crystal frame. Neither nodal force calculations nor mobility laws in the model are coordinate

Table 1
List of reference slip systems for incoming dislocations and GB dislocations for the different possible types of interactions. Sample frames in the simulations are chosen such that the $X$ axis is along the plane normal of the GB (Burgers vector of the GB dislocations for a symmetrical low-angle tilt GB), the $Z$ axis is along the intersection line of the slip plane of the incoming dislocation and the GB plane, and the $Y$ axis is the cross-product of the $X$ and $Z$ axes.

| Incoming dislocation | GB dislocation $1/2[1\,1\,1](0\,1\,\bar{1})$ | Lab frame $X$, $Y$, $Z$ | | |
|---|---|---|---|---|
| $1/2[1\,1\,1](1\,\bar{1}\,0)$ | Collinear | | $[1\,\bar{1}\,0]$ | $[1\,1\,\bar{2}]$ |
| $1/2[1\,\bar{1}\,1](1\,1\,0)$ | Mixed-symmetrical junction | | $[1\,1\,\bar{2}]$ | $[\bar{1}\,1\,0]$ |
| $1/2[1\,\bar{1}\,1](1\,0\,\bar{1})$ | Mixed-asymmetrical junction | $[1\,1\,1]$ | $[1\,0\,\bar{1}]$ | $[\bar{1}\,2\,\bar{1}]$ |
| $1/2[1\,\bar{1}\,1](0\,1\,1)$ | Edge junction | | $[2\,\bar{1}\,\bar{1}]$ | $[0\,\bar{1}\,1]$ |
| $1/2[\bar{1}\,1\,1](0\,1\,\bar{1})$ | Coplanar | | $[0\,1\,\bar{1}]$ | $[\bar{2}\,1\,1]$ |

dependent. However, there are a number of model aspects that are required to identify the Burgers vector and the glide plane of the line segments in a crystal frame. Although the mobility law cannot generally be applied in the crystal reference frame, the mobility of perfect dislocations ($1/2\langle 1\,1\,1\rangle$) and extended dislocations ($\langle 1\,0\,0\rangle$ junctions) are handled differently (see Section 2.2). The use of a cross-slip model allows the glide plane normal of screw segments in the crystal frame to be changed. The dissolution of multi-nodes could lead to a new segment of screw character, whose glide plane is assigned randomly to be one of the cross-slip planes in the crystal reference frame. The calculations of the dislocation flux and the dislocation density vector [27] are required to identify the slip systems. The initial dislocation network used in a laboratory frame simulation should be assigned with Burgers vectors and glide planes in the corresponding laboratory frame instead of the default crystal frame. For this purpose the simulation code was modified to transform the nodal information (Burgers vector, glide plane normal) between crystal and sample frames through rotation operations, as required by the above-mentioned coordinate-dependent model treatments.

### 2.2. Mobility law for $\langle 1\,0\,0\rangle$ dislocations

$\langle 1\,0\,0\rangle$ dislocations in bcc metals are formed as binary interaction products of $1/2\langle 1\,1\,1\rangle$ dislocations. These binary junctions contribute substantially to material strength, provide nucleation sites for axial ternary junctions [8,28], and can bow out to form ternary zigzag configurations [28]. Terentyev et al. [29] have recently started to investigate the core structure and mobility of a straight $[0\,0\,1](1\,\bar{1}\,0)$ edge dislocation and $\langle 1\,0\,0\rangle$ junctions of edge character in bcc iron. The $\langle 1\,0\,0\rangle$ junctions were formed by the interactions between a straight $1/2\langle 1\,1\,1\rangle$ edge or screw dislocation and $1/2\langle 1\,1\,1\rangle$ prismatic loops. Their atomistic simulation results provide a number of insights on how the core structure and mobility of $\langle 1\,0\,0\rangle$ edge dislocations are affected by temperature, which we summarize below:

- A $[0\,0\,1](1\,\bar{1}\,0)$ edge dislocation splits into two perfect $1/2[\bar{1}\,1\,1](1\,\bar{1}\,2)$ and $1/2[1\,\bar{1}\,1](\bar{1}\,1\,2)$ dislocations at $T = 0$ K. The $1/2\langle 1\,1\,1\rangle$ dislocations constrict under a shear stress of 1.5 GPa, which transforms the non-coplanar core to a planar configuration.
- At a temperature below 100 K, the $\langle 1\,0\,0\rangle$ edge dislocation moves via nucleation and propagation of kink pairs, in a similar fashion to the $1/2\langle 1\,1\,1\rangle$ screw dislocation.
- At 300 K and above, the $\langle 1\,0\,0\rangle\{1\,1\,0\}$ edge dislocation behaves in the same manner as a $1/2\langle 1\,1\,1\rangle\{1\,1\,0\}$ edge dislocation, which has a planar core, low Peierls stress and emits elemental kink pairs in the form of $\langle 1\,1\,1\rangle$ crowdions along its core.
- The mobility of the $\langle 1\,0\,0\rangle$ junction of edge character follows the same temperature dependence as the straight $\langle 1\,0\,0\rangle$ edge dislocation. The $\langle 1\,0\,0\rangle$ junction dissociates into two perfect $1/2\langle 1\,1\,1\rangle$ dislocations, when its stability is not favored by the external loading and the motion of other dislocations.

The non-coplanar $\langle 1\,0\,0\rangle$ junctions formed by $1/2\langle 1\,1\,1\rangle$ dislocations on $\{1\,1\,0\}\langle 1\,1\,1\rangle$, $\{1\,1\,2\}\langle 1\,1\,1\rangle$ and $\{1\,2\,3\}\langle 1\,1\,1\rangle$ slip systems are either edge or mixed dislocations, simply because a $\langle 1\,0\,0\rangle$ screw dislocation does not lie on $\{1\,1\,2\}$ and $\{1\,2\,3\}$ planes, and cannot lie on two intersecting $\{1\,1\,0\}$ planes at the same time. Coplanar $\langle 1\,0\,0\rangle$ junctions can zip along any line direction perpendicular to the slip plane normal, which are occasionally of screw character when formed by $1/2\langle 1\,1\,1\rangle$ dislocations on $\{1\,1\,0\}\langle 1\,1\,1\rangle$ slip systems. With these considerations, we extend the above summarized conclusions of Ref. [29] on $\langle 1\,0\,0\rangle$ edge dislocations to $\langle 1\,0\,0\rangle$ dislocations of mixed character, and constrain the motion of $\langle 1\,0\,0\rangle$ screw dislocations to their respective glide planes. The motion of $\langle 1\,0\,0\rangle$ dislocations in DD simulations can be defined through a mobility law applying geometrical constraints (Burgers vector and glide plane normal) in conjunction with temperature-dependent mobility constants.

In ParaDiS v. 2.3.5.1 [6,30], the relation between nodal force and velocity is of the following form[1]:

$$\mathbf{F}_i = \frac{1}{2}\sum_j \|\mathbf{l}_{ij}\|\mathbf{B}_{ij}\mathbf{V}_i, \tag{1}$$

where $\mathbf{F}_i$ is the force on node $i$, $j$ is a node connected to $i$ through a line segment $\mathbf{l}_{ij}$, $\mathbf{B}_{ij}$ is the drag tensor (inverted mobility tensor) for segment $\mathbf{l}_{ij}$, and $\mathbf{V}_i$ is the calculated

[1] This is an approximation that is often used for computational efficiency, see Ref. [6] for details.

nodal velocity. The drag tensor **B** enforces spatial constraints on the dislocation motion according to:

$$\mathbf{B} = \begin{cases} B_g(\mathbf{m}\otimes\mathbf{m}) + B_c(\mathbf{n}\otimes\mathbf{n}) + B_l(\mathbf{t}\otimes\mathbf{t}) & \mathbf{b} = 1/2\langle 1\,1\,1\rangle \\ B_{\langle 100\rangle}\mathbf{I} + (B_l - B_{\langle 100\rangle})(\mathbf{t}\otimes\mathbf{t}) & \mathbf{b} = \langle 1\,0\,0\rangle \end{cases} \tag{2}$$

where the drag coefficient $B_g$ controls dislocation motion on the glide plane and perpendicular to the dislocation line, $B_c$ defines dislocation motion along the glide plane normal **n**, and $B_l$ is the drag coefficient associated with moving a node along its line direction **t**. The drag coefficients can be calculated through the input mobility parameters: $M_{edge}$ (glide mobility of edge dislocations), $M_{climb}$ (climb mobility of edge dislocations) and $M_{screw}$ (mobility of screw dislocations). For an edge segment, $B_g = 1/M_{edge}$ and $B_c = 1/M_{climb}$. For a screw segment, the mobility is isotropic perpendicular to the dislocation line, which means that $B_g = B_c = 1/M_{screw}$. For a segment of mixed character, the drag coefficients are interpolated between the two limits of pure edge and pure screw orientation. $B_l$ is introduced to avoid the singularity of **B**, and is defined as $0.01 \times \mathrm{MIN}(1/M_{edge}, 1/M_{screw})$ to minimize its effect on the mechanical behavior of the system. $B_{\langle 1\,0\,0\rangle}$ was set large enough so that $\langle 1\,0\,0\rangle$ dislocations cannot move perpendicular to the dislocation line. These steps summarize how the nodal velocity is calculated by the mobility law BCC_0 (specific mobility law for bcc crystals implemented in the ParaDiS code). There is another bcc mobility law (BCC_glide) implemented in ParaDiS, which enforces the glide plane constraint on dislocation motion. The nodal velocity $\mathbf{V}_i$ is then projected to $\mathbf{V}_i^{\mathrm{glide}}$ by:

$$\mathbf{V}_i^{\mathrm{glide}} = \mathbf{V}_i - \sum_k (\mathbf{V}_i \cdot \mathbf{norm}_{ik})\mathbf{norm}_{ik}, \tag{3}$$

where $\{\mathbf{norm}_{ik},\ 1 \leqslant k \leqslant 3\}$ is orthogonalized from $\{\mathbf{n}_{ij}, 1 \leqslant j \leqslant 4\}$.

In this work, we modified the drag tensor of $\langle 1\,0\,0\rangle$ dislocations to be the same as that for $1/2\langle 1\,1\,1\rangle$ dislocations (see Eq. (2)), but the drag coefficients $B_g$ and $B_c$ are calculated from a different set of mobility constants: $M_{edge}^{\langle 1\,0\,0\rangle}, M_{climb}^{\langle 1\,0\,0\rangle}$ and $M_{screw}^{\langle 1\,0\,0\rangle}$. The glide plane normal of a non-screw $\langle 1\,0\,0\rangle$ dislocation is the cross-product of its line direction and Burgers vector. A screw $\langle 1\,0\,0\rangle$ dislocation formed by coplanar interaction inherits the glide plane of the parent $1/2\langle 1\,1\,1\rangle$ dislocations. A screw $\langle 1\,0\,0\rangle$ dislocation moves on its original glide plane when generated by the motion of an initially edge or mixed $\langle 1\,0\,0\rangle$ dislocation. Glide plane constraints are enforced through Eq. (3) for both $\langle 1\,0\,0\rangle$ and $1/2\langle 1\,1\,1\rangle$ dislocations, i.e. dislocations cannot leave their glide planes irrespective of their line orientations (edge, mixed and screw).

We now analyze how the mobility of $\langle 1\,0\,0\rangle$ dislocations affects the equilibrium configuration of a ternary dislocation interaction. We consider three dislocations intersecting at their mid-points, namely $1/2[1\,1\,1](0\,1\,\bar{1})$, $1/2[1\,\bar{1}\,1](1\,1\,0)$ and $1/2[\bar{1}\,1\,1](1\,0\,1)$, all of which are initially of edge character, and pinned at both ends (length 2000b) (Fig. 1a). The $1/2[1\,1\,1](0\,1\,\bar{1})$ and $1/2[1\,\bar{1}\,1](1\,1\,0)$ dislocations are attractive and form a mixed-symmetrical junction:

$$1/2[1\,1\,1](0\,1\,\bar{1}) + 1/2[1\,\bar{1}\,1](1\,1\,0) = [0\,1\,0](1\,0\,1).$$

The Burgers vectors of $1/2[\bar{1}\,1\,1](1\,0\,1)$ dislocations (Fig. 1b, c and Fig. 1d, e) are of opposite signs, i.e. they are attractive to $1/2[1\,1\,1](0\,1\,\bar{1})$ dislocation and repulsive to $1/2[1\,\bar{1}\,1](1\,1\,0)$ dislocation (Fig. 1b, c); but repulsive to $1/2[1\,1\,1](0\,1\,\bar{1})$ dislocation and attractive to $1/2[1\,\bar{1}\,1](1\,1\,0)$ dislocation (Fig. 1d, e). Two cases are considered in terms of the mobility ratio between $\langle 1\,0\,0\rangle$ and $1/2\langle 1\,1\,1\rangle$ dislocations: $M^{\langle 100\rangle}/M^{1/2\langle 111\rangle} = 10^{-6}$ (immobile $\langle 1\,0\,0\rangle$ arms) in Fig. 1b, d and $M^{\langle 100\rangle}/M^{1/2\langle 111\rangle} = 1$ (mobile $\langle 1\,0\,0\rangle$ arms) in Fig. 1c, e. A ternary Burgers vector reaction occurs in all cases:

$$1/2[1\,1\,1](0\,1\,\bar{1}) + 1/2[1\,\bar{1}\,1](1\,1\,0) + 1/2[\bar{1}\,1\,1](1\,0\,1) = 1/2[1\,1\,\bar{1}](1\,0\,1).$$

Four different equilibrium configurations are observed, see Fig. 1b–e, which all contain a $1/2[1\,1\,\bar{1}](1\,0\,1)$ ternary junction (second-order junction) and a $[0\,1\,0](1\,0\,1)$ binary junction (first-order junction).

- The $1/2[\bar{1}\,1\,1](1\,0\,1)$ dislocation is attractive to the $1/2[1\,1\,1](0\,1\,\bar{1})$ dislocation and repulsive to the $1/2[1\,\bar{1}\,1](1\,1\,0)$ dislocation:
  - Immobile $[0\,1\,0]$ dislocation, Fig. 1b: the second-order and first-order junctions are coaxial.
  - Mobile $[0\,1\,0]$ dislocation, Fig. 1c: both the binary junction and the ternary junction reorient driven by the interaction between the $1/2[\bar{1}\,1\,1](1\,0\,1)$ dislocation and the $1/2[1\,1\,\bar{1}](1\,0\,1)$ ternary junction.

- The $1/2[\bar{1}\,1\,1](1\,0\,1)$ dislocation is repulsive to the $1/2[1\,1\,1](0\,1\,\bar{1})$ dislocation and attractive to the $1/2[1\,\bar{1}\,1](1\,1\,0)$ dislocation:
  - Immobile $[0\,1\,0]$ dislocation, Fig. 1d: The $1/2[1\,1\,\bar{1}](1\,0\,1)$ ternary junction interacts with the $1/2[\bar{1}\,1\,1](1\,0\,1)$ dislocation, which form a coplanar junction along a different axis from the mixed-symmetrical junction.
  - Mobile $[0\,1\,0]$ dislocation, Fig. 1e: straightening of the binary junction and growing of the ternary junction.

## 3. Simulation results

The incoming dislocations are moving under an uniaxial stress, initially 100 MPa. The loading direction is chosen such that the GB dislocations are free of external stresses and the Schmid factor is 0.41 for the free dislocation slip system. The free dislocations are placed at a distance of 100b from the center of the cubic simulation box (7200b), where the symmetrical low-angle tilt GB is located. When the dislocation motion is impeded by the GB, the applied

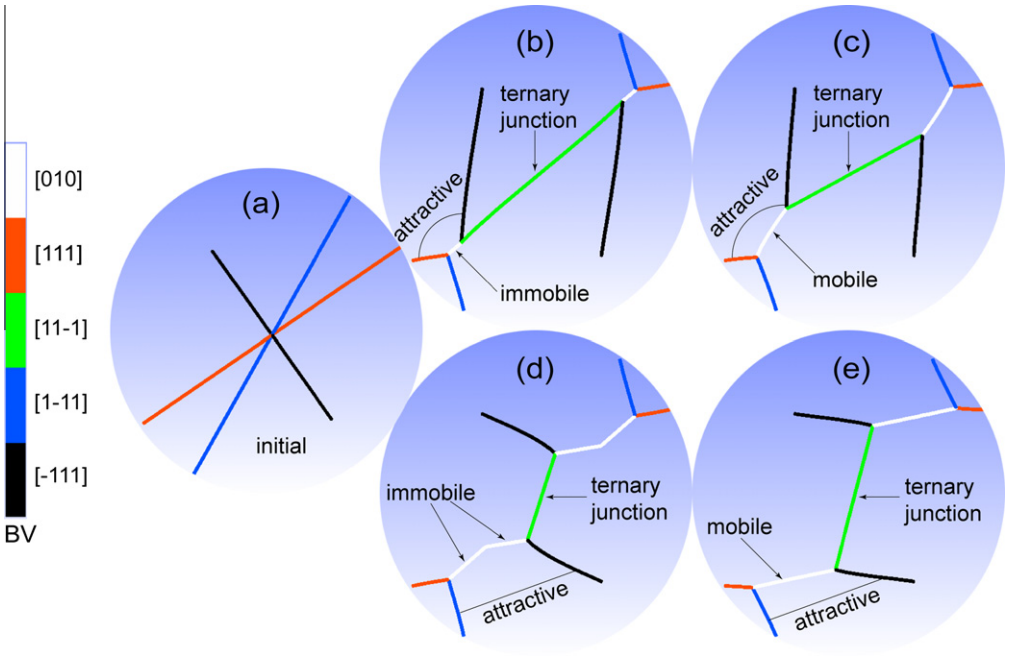


Fig. 1. Overview diagram showing how the mobility of $\langle 100 \rangle$ dislocations affects the equilibrium configuration of a ternary dislocation interaction. (a) Initial $1/2[111](01\bar{1}), 1/2[1\bar{1}1](110)$ and $1/2[\bar{1}11](101)$ dislocations intersect at their mid-points. (b) The $1/2[\bar{1}11](101)$ dislocation is attractive to the $1/2[111](01\bar{1})$ dislocation and repulsive to the $1/2[1\bar{1}1](110)$ dislocation, and the $[010]$ dislocation is immobile. (c) Same as (b) except that the $[010]$ dislocation is mobile. (d) The $1/2[\bar{1}11](101)$ dislocation is repulsive to the $1/2[111](01\bar{1})$ dislocation and attractive to the $1/2[1\bar{1}1](110)$ dislocation, and the $[010]$ dislocation is immobile. (e) Same as (d) except that the $[010]$ dislocation is mobile. A ternary junction is formed by $1/2[111](01\bar{1}) + 1/2[1\bar{1}1](110) + 1/2[\bar{1}11](101) = 1/2[11\bar{1}](101)$. Mixed-symmetrical junction: $1/2[111](01\bar{1}) + 1/2[1\bar{1}1](110) = [010](101)$. Coplanar junction: $1/2[\bar{1}11](101) + 1/2[11\bar{1}](101) = [010](101)$. BV: Burgers vector.

stress is gradually increased to retain the initial strain rate. ParaDiS uses isotropic elasticity. The shear modulus (82 GPa), Poisson ratio (0.29) and Burgers vector are chosen to represent bcc iron. The mobility parameters are used for dislocation motion at elevated temperatures, $M_{edge} = M_{screw} = 1\ \mathrm{Pa}^{-1}\ \mathrm{s}^{-1}$. The dislocation spacing in the GB is 100b, and the dislocation lines are discretized with segments of length in the range from 15b to 50b. The incoming dislocation is periodically extended. The GB dislocations are pinned at their ends for non-coplanar interactions, and periodically extended when the incoming dislocation and GB dislocation are coplanar. Both positive and negative incoming dislocations are investigated. The reference slip systems of the incoming dislocations and the GB dislocations used in the numerical simulations are listed in Table 1, together with the sample frames used for studying the different types of dislocation interactions.

When considering $\{110\}\langle 111 \rangle$ slip systems, an incoming dislocation intersects a symmetrical low-angle tilt GB at either edge or mixed orientations (sample axis $Z$ in Table 1). The free dislocation penetration of the interface does hence not involve any cross-slip of screw dislocations. For this reason the cross-slip capability is disabled in the current version of the model.

The stress–strain curves are given in Fig. 2, for the case where the simulations assume that the incident dislocations and the GB dislocations are on intersecting slip planes. Negative incident dislocations on collinear slip systems

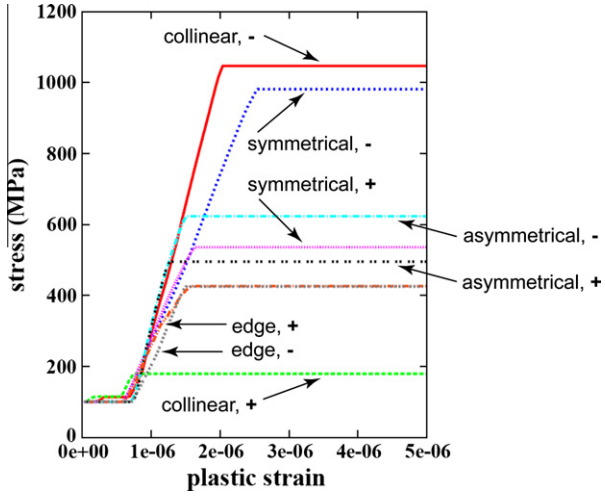


Fig. 2. Stress–strain curves for the case where the incident dislocations and the GB dislocations are on intersecting slip planes. We consider collinear (collinear slip system), symmetrical (mixed-symmetrical junction forming slip system), asymmetrical (mixed-asymmetrical junction forming slip system) and edge (edge junction forming slip system) configurations. The symbol "+" refers to a positive incident dislocation, and "−" to a negative incident dislocation. The loading direction is chosen such that the GB dislocations are free of external stresses and the Schmid factor is 0.41 for the incident dislocation slip system. The incoming dislocations are moving under a uniaxial stress, initially 100 MPa. When the dislocation motion is impeded by the GB, the applied stress is gradually increased to retain the initial strain rate.

and mixed-symmetrical junction forming slip systems have the most difficulty in penetrating the symmetrical low-angle tilt GB. In both cases, Burgers vector reactions are observed. The incident dislocations on mixed-asymmetrical junction and edge junction forming slip systems do not form binary junctions with the GB dislocations, but form crossed states when the incident and GB dislocations are attracted towards each other. The incident dislocation and the GB dislocations on the collinear slip systems are partially annihilated (the screw parts), and the rest of the incident dislocation is rendered into short segments with both ends connected to the GB dislocations (Fig. 3a). Upon increasing the external stress to 1047 MPa, the short segments bow out and recombine (Fig. 3b). Both the initial partial annihilation and the latter recombination involve the annihilation of two arrays of screw segments. Note that for the case of a collinear interaction, both the incoming dislocation and the GB dislocations are initially of edge character. An array of mixed-symmetrical junctions is formed by the interactions between the GB dislocations and the incident dislocation, $1/2[1\,1\,1](0\,1\,\bar{1}) + 1/2[1\,\bar{1}\,1](1\,1\,0) = [0\,1\,0](1\,0\,1)$ (Fig. 4a). These mixed-symmetrical junctions dissociate when the external stress reaches 981 MPa (Fig. 4b). When comparing Fig. 4b with Fig. 4a, we observe that the incident dislocation moves downwards when still attached to the GB. To further investigate this phenomenon, we simulate the incoming dislocation pile-ups on the mixed-symmetrical junction forming slip system. Four incoming dislocations are placed at the front of the GB at a distance of 100b, 200b, 300b and

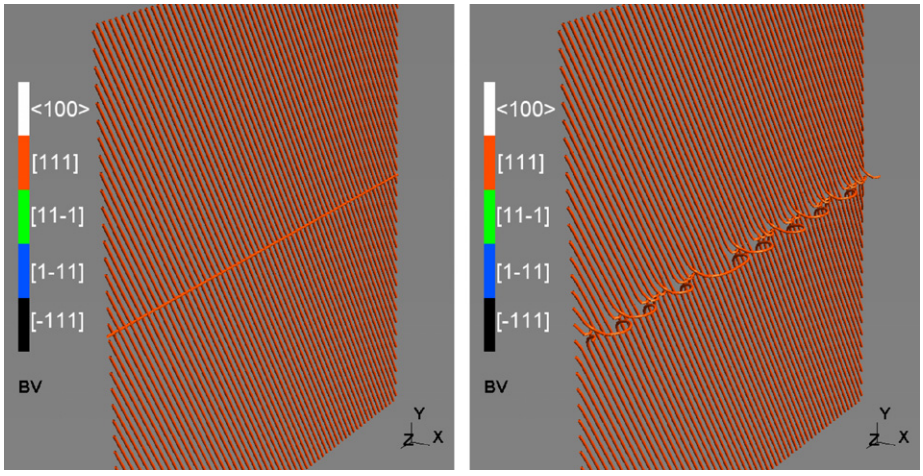


(a) partially annihilated (b) bow out and recombine

Fig. 3. Collinear annihilation between the incident dislocation and GB dislocations. Both the initial partial annihilation and the latter recombination involve the annihilation of two arrays of screw segments. BV: Burgers vector.

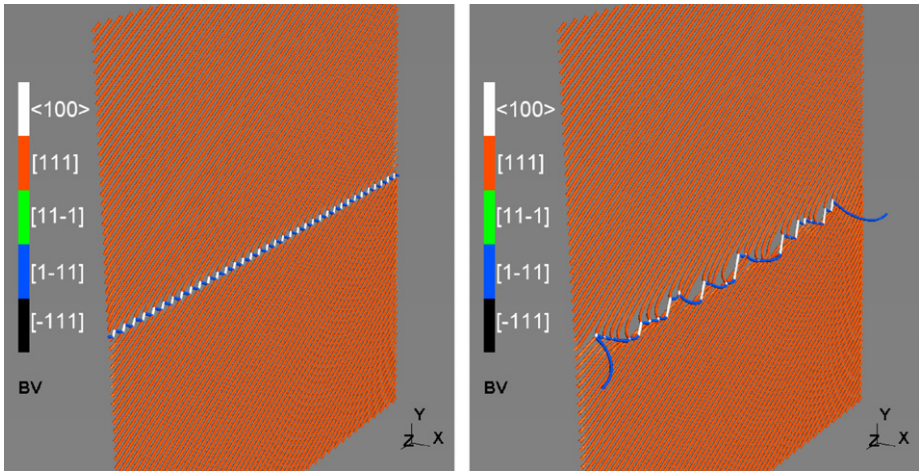


(a) an array of mixed-symmetrical junctions (b) junction dissolution

Fig. 4. Mixed-symmetrical junction formation between the incident and the GB dislocations, $1/2[1\,1\,1](0\,1\,\bar{1}) + 1/2[1\,\bar{1}\,1](1\,1\,0) = [0\,1\,0](1\,0\,1)$. BV: Burgers vector.

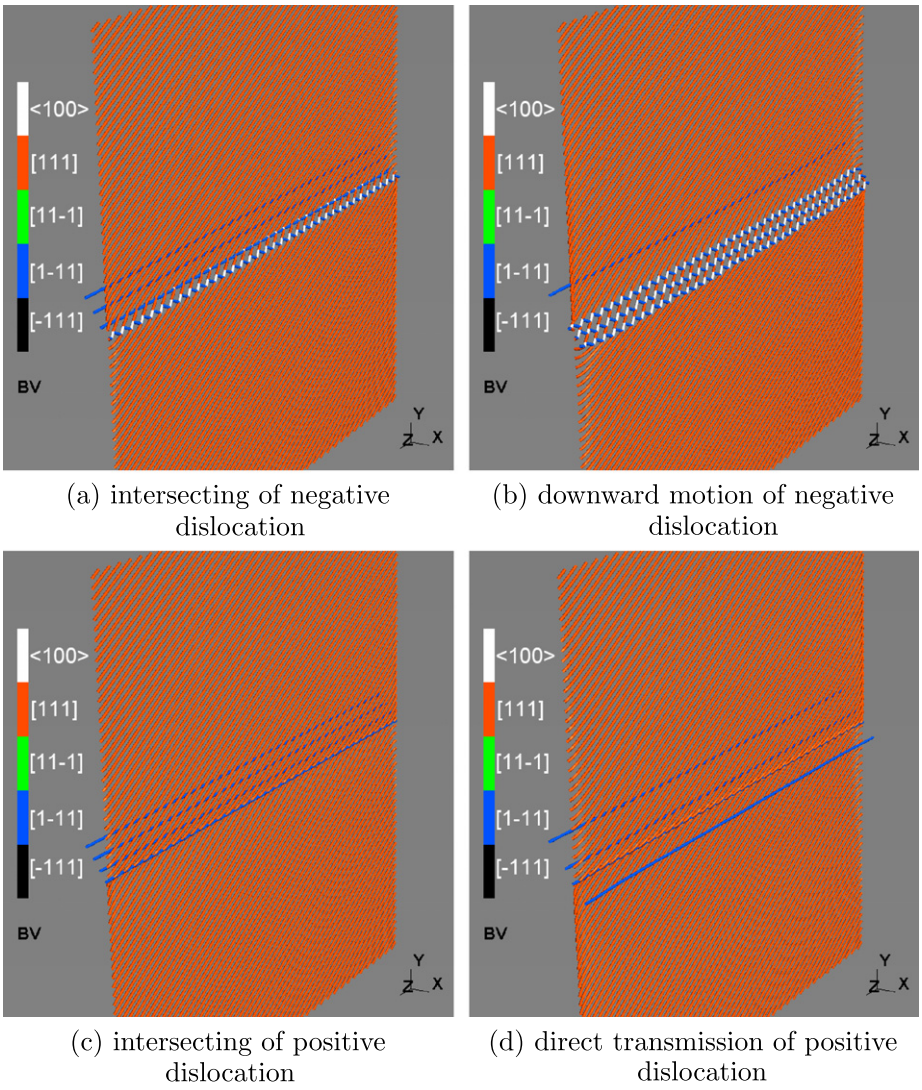


(a) intersecting of negative dislocation

(b) downward motion of negative dislocation

(c) intersecting of positive dislocation

(d) direct transmission of positive dislocation

Fig. 5. Pile-up of the incident dislocations on the mixed-symmetrical junction forming slip system. The negative leading dislocation has already moved downwards from its initial incident position, when the following dislocations touch the GB. A hexagonal network is generated, which is associated with the bending of the GB dislocations. BV: Burgers vector.

400b, respectively, all of which are on the same slip plane. In Fig. 5a, the negative leading incident dislocation forms mixed-symmetrical junctions with the GB dislocations. The leading dislocation has already moved downwards from its initial incident position when the following dislocations touch the GB (Fig. 5b). A hexagonal network is generated, which is associated with the bending of the GB dislocations. The downward motion is not observed for the positive incident dislocation (Fig. 5c), and the leading dislocation penetrates the GB from its initial intersections under an external stress of 142 MPa (Fig. 5d). If the mobility ratio $M^{\langle 100\rangle}/M^{1/2\langle 111\rangle}$ is increased from $10^{-6}$ to 1, the transmission resistance for single dislocation drops from 981 to 775 MPa, but rises from 667 to 778 MPa for the leading dislocation in the hexagonal network (pile-up case).

The stress–strain response results are shown in Fig. 6, for the case where the incident dislocation and the GB dislocations are in coplanar interaction. Both the contact interaction (same slip plane) and the non-contact interaction (parallel slip planes) are considered. The negative dislocation encounters a GB dislocation, both of which combine into a coplanar junction. Depending on the mobility of the coplanar junction, it remains in the GB as a foreign dislocation (immobile $\langle 100\rangle$ dislocation), or glides away and leaves behind an opening in the GB (mobile $\langle 100\rangle$ dislocation) (Fig. 7a). The positive dislocation pushes a GB dislocation out of the GB when the external stress is increased to 957 MPa (Fig. 7b).

## 4. Discussion

The transmission resistance values for incoming dislocations through a symmetrical low-angle tilt GB ($\theta = 0.57°$) have been quantified in terms of the different types of interactions between the incoming and GB dislocations. The

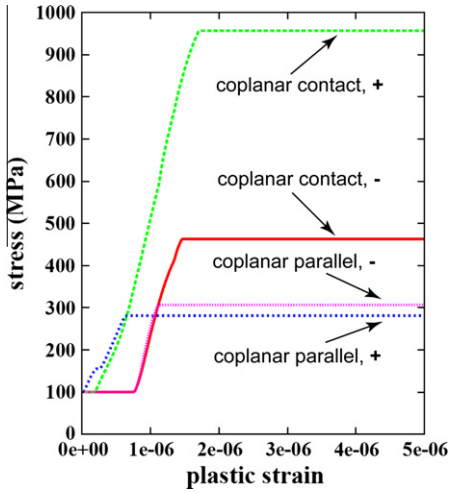


Fig. 6. Stress–strain curves for the case where the incident dislocations and the GB dislocations are on coplanar slip systems. Contact interaction (same slip plane) and non-contact interaction (parallel slip plane). The symbol "+" refers to positive incident dislocations, and "−" to negative incident dislocations. The loading direction is chosen such that the GB dislocations are free of external stresses and the Schmid factor is 0.41 for the incident dislocation slip system. The incoming dislocations are moving under a uniaxial stress, initially 100 MPa. When the dislocation motion is impeded by the GB, the applied stress is gradually increased to maintain the initial strain rate.

strengthening effects associated with these different interactions deviate significantly from the average interaction strengths in the context of forest hardening [21,25]. This is related to the special contact geometry between the incoming dislocations and the GB dislocations, and the fact that the GB dislocations tend to stay at their energetically favored positions. The incident dislocation and the GB dislocations on collinear slip systems repel each other with the weakest interaction force among all cases considered. When the collinear annihilation does not occur, the transmission resistance amounts to 179 MPa for the positive incident dislocation. For the negative incident dislocation, screw parts of the dislocation are annihilated, and the remaining segments require an external stress of 1047 MPa to bow out and recombine. For the incoming dislocations on the three non-coplanar junction forming slip systems, the combination with GB dislocations to form mixed-asymmetrical and edge junctions has not been observed. For these two cases, the transmission resistances of the crossed state and the repulsive interaction are close to each other. We observed that the most important interaction happens when the incident dislocation and the GB dislocations are on mixed-symmetrical junction forming slip systems. The GB absorbs the negative incident dislocation by forming an array of binary junctions. When the external force and the repulsive force from pile-up dislocations are not high enough to break the binary junctions, the absorbed incident dislocations move downwards and form a hexagonal network. This finding reveals that a hexagonal network (a general low-angle GB) can be generated by mixed-symmetrical junction formation events of the incident dislocations and a symmetrical low-angle tilt GB, even when the incoming dislocations are originally in a pile-up arrangement.

Dislocations are situated close together in low-angle grain boundaries, and coplanar interactions with the incoming dislocations occur more often on the same slip plane. The positive incident dislocation requires an external stress of 957 MPa to push a GB dislocation out of the symmetrical low-angle GB ($\theta = 0.57°$). The negative incident dislocation merges entirely with one of the GB dislocations. The corresponding transmission strength is determined by the mobility of the $\langle 100 \rangle$ dislocation. Mobile $\langle 100 \rangle$ mixed-symmetrical junctions are found to let the single incident dislocation transmit more easily through the interface, but make it more difficult for the dislocations in a partial pile-up arrangement to leave a hexagonal network.

Although transmission resistance is the key factor underlying GB strengthening, the individual interactions between free dislocations and grain boundaries are a more

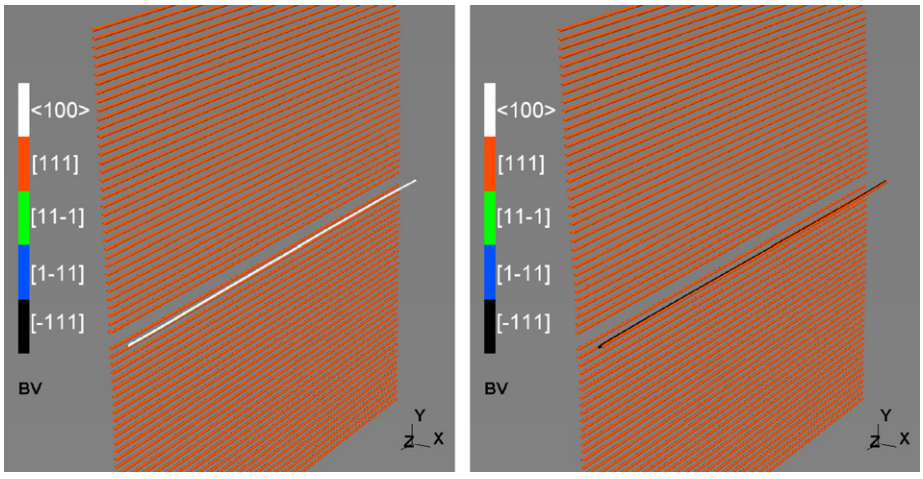


(a) attractive (b) repulsive

Fig. 7. The incident dislocation and one GB dislocation are on the same slip plane.

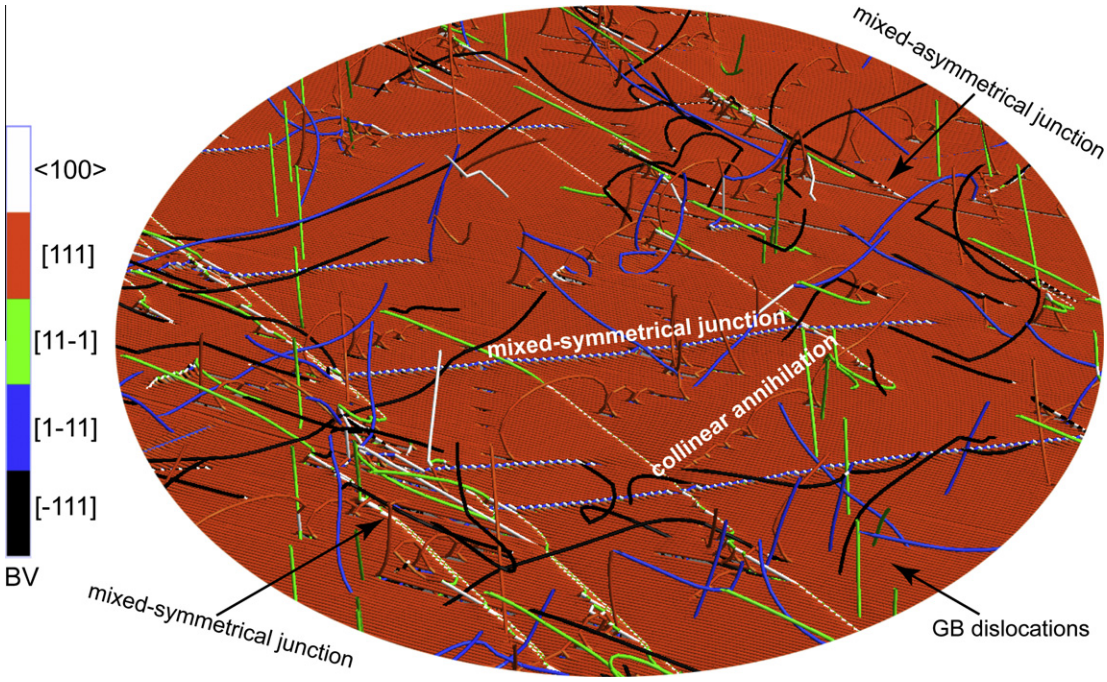


Fig. 8. A simulation snapshot cut in the vicinity of the symmetrical low-angle tilt GB ($\theta = 0.57°$). Free dislocations are generated from 48 Frank–Read sources (edge, screw, positive and negative segments) on 12 $\{1\,1\,0\}\langle 1\,1\,1\rangle$ slip systems. Eight slip systems are activated with respect to the GB dislocation slip system: two are collinear slip systems, two are mixed-symmetrical junction forming slip systems, and the other four are mixed-asymmetrical junction forming slip systems.

complicated configuration problem. The low-angle GB can affect the multiplication of curved free dislocations and hence the entire dislocation structure evolution in the system. We therefore also simulated the interaction between a symmetrical low-angle tilt GB ($\theta = 0.57°$) and free dislocations generated from 48 Frank–Read sources (edge, screw, positive and negative segments) on 12 $\{1\,1\,0\}\langle 1\,1\,1\rangle$ slip systems. The Frank–Read sources have equal lengths (3500b, $\tau_0 = 23$ MPa), and are randomly distributed in a cubic simulation box (35,000b). A constant tensile strain rate of 10 $s^{-1}$ is applied ($\sigma_{max} = 416$ MPa). Eight slip systems are simultaneously activated by the external loading with respect to the GB dislocation slip system: two are collinear slip systems, two are mixed-symmetrical junction forming slip systems, and the other four are mixed-asymmetrical junction forming slip systems. A simulation snapshot cut in the vicinity of the GB is shown in Fig. 8. For curved dislocations in a more complex environment, the negative incident dislocations on mixed-symmetrical junction forming slip systems are also absorbed by the GB, and form long arrays of binary junctions, very similar to straight dislocations. Mixed-asymmetrical junctions are observed for curved incident dislocations in some locations, where the junction formation is favored by the local interactions with other free dislocations in the neighborhood. Collinear annihilations do not occur at the tips of the curved dislocations, but at the two sides. Partial transmission is commonly observed for the case of curved incident dislocations on collinear slip systems. The simulation results obtained on curved dislocations will be analyzed in more detail in a separate publication, together with a study of the GB's role on dislocation multiplication and dislocation structure evolution.

## 5. Concluding remarks

We investigated the transmission resistance associated with a symmetrical low-angle tilt GB ($\theta = 0.57°$) in terms of the different interaction strengths between the incident and GB dislocations. In this fixed contact geometry, the collinear interaction is the weakest one in terms of the interaction force, but can strongly impede dislocation motion when partial annihilations are involved. Combination of the incident and GB dislocations to form mixed-asymmetrical and edge junctions has not been observed, and the transmission resistances of the crossed state and the case of repulsive interaction are close to each other. We found that the most important interaction happens when the incident dislocation and the GB dislocations are on mixed-symmetrical junction forming slip systems. Interactions of this type not only cause a strong resistance against the incident dislocation penetration, but also transform the symmetrical low-angle tilt GB into a hexagonal network (a general low-angle GB).

Further we observed that the mobility of the $\langle 1\,0\,0\rangle$ dislocation controls the behavior of the coplanar junction (single $\langle 1\,0\,0\rangle$ dislocation) formed by incident and GB dislocations. Mobile $\langle 1\,0\,0\rangle$ mixed-symmetrical junctions are found to let the single incident dislocation transmit more easily (an array of $\langle 1\,0\,0\rangle$ dislocations), but make it more

difficult for the dislocations in a partial pile-up arrangement to leave a hexagonal network (arrays of ⟨100⟩ dislocations). We also discussed how the mobility of a ⟨100⟩ dislocation affects the equilibrium configuration of a ternary dislocation interaction. The mobility of ⟨100⟩ binary junctions affects their own strength and the way they interact with 1/2⟨111⟩ dislocations to form second-order junctions.

## Acknowledgments

Some results addressed in this paper have been achieved using the PRACE Research Infrastructure Blue Gene/P located in Germany at the Jülich Supercomputing Centre through the grant (PRA025) 'A dislocation dynamics study of dislocation cell formation and interaction between a low angle grain boundary and an incoming dislocation'.

## Appendix A. Supplementary material

Supplementary data associated with this article can be found, in the online version, at doi:10.1016/j.actamat.2011.07.067.

## References

[1] Kubin LP, Canova G, Condat M, Devincre B, Pontikis V, Brechet Y. Solid State Phenom 1992;23–24:455–72.
[2] Zbib HM, Rhee M, Hirth JP. Int J Mech Sci 1998;40(2–3):113–27.
[3] Schwarz KW. J Appl Phys 1999;85(1):108–19.
[4] Ghoniem NM, Tong SH, Sun L. Z Phys Rev B 2000;61(2):913–27.
[5] Weygand D, Friedman LH, Van der Giessen E, Needleman A. Modell Simul Mater Sci Eng 2002;10(4):437–68.
[6] Arsenlis A, Cai W, Tang M, Rhee M, Oppelstrup T, Hommes G, et al. Modell Simul Mater Sci Eng 2007;15(6):553–95.
[7] Madec R, Devincre B, Kubin LP, Hoc T, Rodney D. Science 2003;301(5641):1879–82.
[8] Bulatov VV, Hsiung LL, Tang M, Arsenlis A, Bartelt MC, Cai W, et al. Nature 2006;440(7088):1174–8.
[9] Uchic MD, Dimiduk DM, Florando JN, Nix WD. Science 2004;305(5686):986–9.
[10] Rao SI, Dimiduk DM, Parthasarathy TA, Uchic MD, Tang M, Woodward C. Acta Mater 2008;56(13):3245–59.
[11] El-Awady JA, Biner SB, Ghoniem NM. J Mech Phys Solids 2008;56(5):2019–35.
[12] Tang H, Schwarz KW, Espinosa HD. Phys Rev Lett 2008;100(18).
[13] Senger J, Weygand D, Gumbsch P, Kraft O. Scripta Mater 2008;58(7):587–90.
[14] El-Awady JA, Wen M, Ghoniem NM. J Mech Phys Solids 2009;57(1):32–50.
[15] Devincre B, Hoc T, Kubin LP. Science 2008;320(5884):1745–8.
[16] Devincre B, Kubin LP, Hoc T. Scripta Mater 2006;54(5):741–6.
[17] Csikor FF, Motz C, Weygand D, Zaiser M, Zapperi S. Science 2007;318(5848):251–4.
[18] Wickham LK, Schwarz KW, Stolken JS. Phys Rev Lett 1999;83(22):4574–7.
[19] Madec R, Devincre B, Kubin LP. Comput Mater Sci 2002;23(1-):219–24.
[20] Dupuy L, Fivel MC. Acta Mater 2002;50(19):4873–85.
[21] Madec R, Kubin LP. In: Kitagawa H, Shibutani Y, editors. IUTAM symposium on mesocopic dynamics of fracture process and materials strength (Osaka, Japan). Dordrecht: Kluwer Academic Publishers; 2004. p. 69–78.
[22] Bulatov V, Abraham FF, Kubin LP, Devincre B, Yip S. Nature 1998;391(6668):669–72.
[23] Shenoy VB, Kukta RV, Phillips R. Phys Rev Lett 2000;84(7):1491–4.
[24] Franciosi P, Berveiller M, Zaoui A. Acta Metall 1980;28(3):273–83.
[25] Queyreau S, Monnet G, Devincre B. Int J Plast 2009;25(2):361–77.
[26] Cai W, Arsenlis A, Weinberger CR, Bulatov VV. J Mech Phys Solids 2006;54(3):561–87.
[27] Hartley CS, El-Awady JA, Liu B, Woodward C, Raabe D, in preparation.
[28] Madec R, Kubin LP. Scripta Mater 2008;58(9):767–70.
[29] Terentyev DA, Osetsky YN, Bacon D. J Acta Mater 2010;58(7):2477–82.
[30] Documentation of ParaDiS v2.3.5.1.